Taylor & Francis
Taylor & Francis Group

Vehicle System Dynamics
International Journal of Vehicle Mechanics and Mobility

ISSN: (Print) (Online) Journal homepage: www.tandfonline.com/journals/nvsd20

Modelling and application of yaw damper with frequency-selective damping on railway vehicles

Xiaoxing Deng, Yan Zhou, Xiangwang Chen, Yuan Yao & Longjiang Shen

VEHICLE SYSTEM DYNAMICS
https://doi.org/10.1080/00423114.2024.2445761

Modelling and application of yaw damper with frequency-selective damping on railway vehicles

Xiaoxing Deng[a,b], Yan Zhou[a], Xiangwang Chen[a], Yuan Yao [a] and Longjiang Shen[b]

[a]State Key Laboratory of Rail Transit Vehicle System, Southwest Jiaotong University, Chengdu, People's Republic of China; [b]State Key Laboratory of Heavy-Duty and Express High-Power Electric Locomotive, CRRC Zhuzhou Electric Locomotive Co., Ltd., Zhuzhou, People's Republic of China

ABSTRACT

In this study, a new mechanical yaw damper with frequency-selective damping (FSD) is investigated. The structure principle, modelling and simulation of the damper and its core component, the frequency-selective damping valve, are elaborated. Compared with the conventional damper, the static and dynamic characteristics of the FSD damper have been tested in the experimental bench, and the damping variation rate is proposed to evaluate the damping force variation. A physical parameter model of the yaw damper is established by using the AMESim software, and the simulation accuracy has been verified by comparing the simulated results with the experimental ones. A detailed analysis has been performed for the influence of key parameters of the FSD valve on the mechanical characteristics of the FSD damper. Finally, through the AMESim/Simpack co-simulation method, the dynamic performances of a high-speed locomotive equipped with the FSD yaw damper have been simulated. The results indicate that the FSD yaw damper improves the adaptive stability of railway vehicles in different wheel–rail matching states. In addition, the dynamic performance of the vehicle can be improved when passing through the turnout and narrow curves.

ARTICLE HISTORY
Received 8 June 2024
Revised 4 October 2024
Accepted 17 December 2024

KEYWORDS
Railway vehicle; adaptive stability; yaw damper; frequency-selective damping; wheel–rail relationship

1. Introduction

With the continuous increase of operating speed and mileage, the dynamic interaction between wheel and rail, as well as the dynamic loading of railway vehicles have been enhanced, which lead to increasingly serious and complex issues on vehicles. The suspension components with fixed parameters selected through multi-objective optimisation no longer satisfy the requirements of vehicle dynamics performance under various complex working conditions. With the development of technology, the application of variable-parameter suspension components will prevail on railway vehicles [1–5]. The suspension parameters can be automatically adjusted according to the working states of the damper, such as the stroke, speed and action frequency, through its internal mechanical structure. This kind of variable-parameter damper can ensure its reliability without any complex external control system [6–9]. The application of this type of suspension system can

CONTACT Longjiang Shen shenlongjiang.zz@crrcgc.cc

make the railway vehicle more intelligent and adaptable under complex operating conditions, improving the vehicle running safety, hunting stability and ride comfort. Therefore, variable-parameter suspension technology is of great value to engineering applications in railway vehicles.

The mechanical variable-parameter damper realises the real-time adjustment of damping or dynamic stiffness automatically through its internal mechanical elements according to the working state. In essence, it changes the flow area of the oil circulation inside the damper. At present, there are mainly two types of mechanical variable-parameter dampers with relatively mature technology. One is the displacement-related damper, and the other is the frequency-sensitive damper. The former adjusts the damper parameters automatically according to the stroke, and the latter adjusts the dynamic characteristics of the damper according to the acting frequency [10,11]. The frequency-sensitive type damper can be further divided into frequency-selective damping (FSD) damper and frequency-selective stiffness (FSS) damper. Paul de Kortschak [12] from KONI Company in the Netherlands invented a fluid-filled frequency-dependent damper, which can achieve the characteristics of small damping at low frequencies and large damping at high frequencies. One application example is the frequency-selective yaw damper for railway vehicles, such as the 1016 series locomotive in Austrian National Railway. It is installed between the bogie and the carbody in the longitudinal direction to settle the contradiction in the damping requirement for two operating conditions: passing narrow curves and high-speed running on straight lines.

The mechanical characteristics exhibited by the FSD or FSS damper are in line with the requirements of the railway vehicle for yaw dampers. Therefore, in recent years, the frequency-dependent parameter damper has gradually become a research hotspot. In 2022, Cheng [13] proposed to replace the conventional yaw damper with the FSD yaw damper to solve the problem of low-frequency carbody swaying of high-speed locomotives. The research results showed that the frequency-dependent damping yaw damper could significantly reduce the peak values of the lateral vibration acceleration and yaw angular acceleration of the carbody. In 2023, Huo [14] compared the FSS yaw damper with two conventional yaw dampers. Through numerical simulations and bench tests, it was found that the FSS yaw damper could improve the adaptability of the lateral stability of the railway vehicle to low/high wheel–rail contact conicity. In 2023, aiming at the robustness and adaptive stability of the wheel–rail contact geometric relationship of high-speed trains, Yao [15] summarised the matching rules of bogie suspension parameters, clarified the influence mechanism of the dynamic stiffness of yaw damper on the lateral stability of the vehicle, and proposed the requirements of the frequency-dependent stiffness of the yaw damper. In 2023, in order to increase the high-speed stability and curve passing ability of high-speed trains, Isacchi [16] applied the FSD yaw damper to high-speed trains. Compared with the vehicle equipped with a passive yaw damper, the wheel–rail lateral force, derailment coefficient and wheel wear index of passing through a S-curve were all reduced after using the FSD yaw damper. Meanwhile, the stability during high-speed operation can be ensured. In 2023, Li [11] proposed to use the FSD yaw damper to replace the original yaw damper to solve the problem that the conventional yaw damper could not balance the lateral stability of a high-speed locomotive in high/low equivalent conicity conditions, and the application effect of the frequency-dependent damping yaw damper was studied through dynamic simulation.

At present, most relevant literature conducted research on vehicle dynamics based on the description of the mechanical characteristics of the external frequency-dependent parameters of the yaw damper, without involving the internal structure principle, modelling method, and analysis of the influence of specific structural parameters. In this paper, taking a real mechanical FSD yaw damper produced by KONI Company as the research object, the structure composition, and working principle of its core element, the FSD valve, are analysed. The static and dynamic characteristics tests of the conventional and FSD yaw dampers are carried out, respectively, and the differences in the force-displacement hysteresis curve are compared. It is proposed to use the damping variation rate to evaluate the damping changing of the FSD damper. According to the actual structure of patent disclosure [8,12], a physical parameter model of the yaw damper is established in the AMESim software, and the accuracy of the established model is verified by the damper sample testing. The influence of key parameters of the FSD valve on the mechanical characteristics of the yaw damper is analysed in detail. Finally, a co-simulation model of a high-speed locomotive incorporating the FSD yaw damper is established using the AMESim and Simpack software. Through the simulation, it is verified that the FSD yaw damper can improve the adaptability of the locomotive to different wheel–rail contact states. In addition, it can reduce the wheel–rail wear when the railway vehicle passes through the turnout and narrow curves.

2. Structure principle of FSD valve

The hydraulic damper can be divided into single-cycle damper and double-cycle damper according to the oil flow direction [17]. No matter whether in the rebound or compression stroke, the internal oil passes through various damping valves to produce the damping force, converting kinetic energy into heat energy, so as to dissipate vibration energy [18]. Different from the conventional damper, the FSD yaw damper includes a pair of FSD valves added to the piston, with which the mechanical characteristics can be automatically adjusted according to the action frequency and even the piston stroke. In this study, a double-cycle yaw damper incorporating the FSD valve produced by KONI Company in the Netherlands is taken as the investigation object, and its mechanical characteristics and structural principle are analysed.

The FSD valve is a key component for achieving the damping force variation in the hydraulic damper. The FSD valve closes at high frequencies, which leads to the mechanical characteristic consistent with that of a conventional damper and maintains a high damping force. On the contrary, the FSD valve opens when the action frequency is lower than the critical value, increasing the flow area on the piston and thus reducing the generated damping force. The opening or closing of the FSD valve is automatically switched by its mechanical structure. The FSD valve mainly consists of a valve body, a first auxiliary chamber, an auxiliary piston, a second auxiliary chamber, a spring, and sealing devices, etc., as shown in Figure 1. According to the patent disclosure [12], the auxiliary piston also includes a constant orifice, a check valve and a sealing ring. Two FSD valves are installed in reverse on the piston. One is called the rebound FSD valve, which is connected to the rebound chamber and works during the rebound stroke, and the other is called the compression FSD valve, which is connected to the compression chamber and works during the compression stroke.

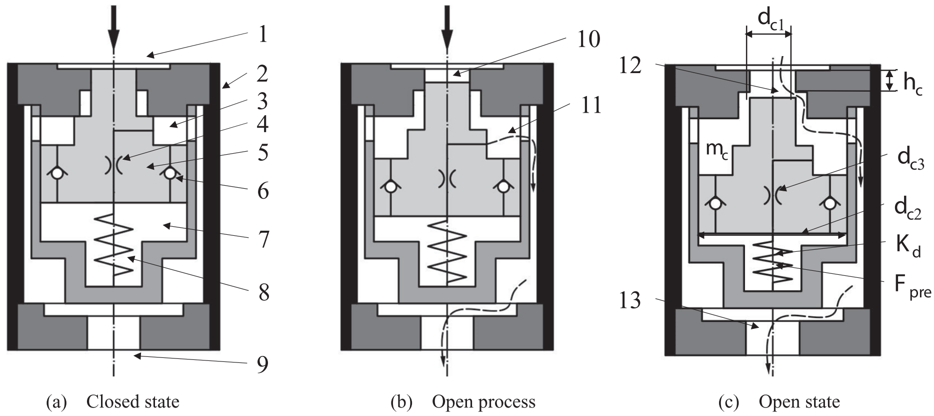

Figure 1. Structure and working process of the FSD valve [12]. (a) Closed state; (b) Open process; (c) Open state. 1-Rebound chamber; 2-Valve body; 3-First auxiliary chamber; 4-Constant orifice; 5-Auxiliary piston; 6-Check valve; 7-Second auxiliary chamber; 8-Spring; 9-Compression chamber; 10-Auxiliary piston upper orifice; 11,12,13-Directions of oil flow.

Specifically, the rebound FSD valve closes at small strokes and high action frequencies, as shown in Figure 1(a). During the rebound stroke, the hydraulic pressure in the rebound chamber is much greater than that in the compression chamber and the second auxiliary chamber. However, due to the small diameter of the constant orifice on the auxiliary piston, the hydraulic fluid in the second auxiliary chamber cannot flow out in an extremely short time. It renders the amplitude of the auxiliary piston downwards within one cycle less than the height at the upper orifice (named boss height), thus keeping the FSD valve closed. Consequently, the damper exhibits a high damping force at this moment. After the action frequency decreases, the downward displacement of the auxiliary piston increases, showing a tendency to open, as depicted in Figure 1(b). In the state of large amplitude and low frequency, there is sufficient time for hydraulic oil in the second auxiliary chamber to flow out through the constant orifice and enter the first auxiliary chamber and the compression chamber. The direction of oil flow is indicated by arrow 11. After the oil flows out, the auxiliary piston can move downwards. If the downward displacement of the auxiliary piston within a single cycle exceeds the boss height, the FSD valve will open, as shown in Figure 1(c). At this point, the hydraulic fluid in the rebound chamber of the damper can flow through the auxiliary piston upper orifice and reach the compression chamber, as indicated by arrows 12 and 13. The effective area of the orifice on the piston increases, resulting in a low damping force at this stage. In the reverse direction, the check valve opens and the hydraulic oil can quickly return to the second auxiliary chamber, causing the FSD valve to quickly close to eliminate the impact on the damping force in the compression stroke.

3. Mechanical characteristics testing

The test subjects include the conventional double-cycle yaw damper and the FSD yaw damper. The static and dynamic mechanical characteristic comparison has been made between these two types of dampers based on EN 13802-2013 [19].

3.1. Static characteristics

From the analysis of Section 2, it can be inferred that there is a certain delay in the opening process of the FSD valve. The static characteristic test mainly focuses on the variation of damping force after the FSD valve opens. In the bench test, a large-amplitude and low-frequency sinusoidal displacement excitation was adopted, generally with an amplitude of 25 mm and an excitation frequency below 2 Hz [19]. The static test results of the conventional and the FSD damper are shown in Figure 2. The hysteresis loops of the conventional damper are full and smooth, and they exhibit clear unloading characteristics. The unloading force is approximately 16 kN. After reaching the unloading force, the damping force increases gradually with the velocity and reaches a maximum of around 20 kN. Comparing Figure 2(a) and (b), it can be observed that in the initial segment of the rebound-compression switch, the damping forces of the two dampers are consistent, and the curves basically overlap. This phenomenon is due to the delay in opening of the FSD valve; it is still closed at this point. With the increase in amplitude, the damping force of the FSD damper decreases rapidly, since the FSD valve has opened, resulting in an increase in flow area between the compression chamber and the rebound chamber. When the action frequency is below 2 Hz, there is a clear damping force reduction of the FSD damper. Meanwhile, with the increase in action frequency, the delay of the FSD valve opening and the corresponding damping force gradually increase.

Figure 2(c) compares the force-velocity characteristic curve of the conventional damper and FSD damper working under the two different conditions of the FSD valve. It can be observed that the maximum damping force of the FSD damper is consistent with that of the conventional damper when the FSD valve is closed, while it is remarkably reduced after the FSD valve opens.

3.2. Dynamic characteristics

To gain a deeper understanding of the characteristics of the FSD damper, the dynamic characteristic tests were further conducted, and comparisons were made with the conventional damper. The dynamic test involves a smaller amplitude, typically ranging from 0.2 to 4 mm, and the action frequencies between 0.5 and 15 Hz. Considering that the required switching frequency of the FSD valve is about 2–3 Hz, emphasis was placed on analysing the hysteresis curves at excitation frequencies below 5 Hz. The dynamic test results of the conventional and the FSD dampers at amplitudes of 2.0 and 4.0 mm are shown in Figure 3. Both dampers reach the unloading force, exhibiting clear unloading characteristics, and their hysteresis loops tend towards a quadrilateral shape. When the excitation frequency is 2 Hz or below, there is a significant difference between the hysteresis loops of the two dampers. The damping force of the FSD damper shows a significant decrease in the middle and later stages of both rebound and compression strokes, indicating that the FSD valve is open at the moment. This phenomenon is more pronounced at the amplitude of 4.0 mm. Meanwhile, the proportion of the small damping force segment decreases as the excitation frequency increases. When the excitation frequency is above 3 Hz, there is no reduction in the damping force for the FSD damper, and its hysteresis loop is basically consistent with that of the conventional damper, indicating that the FSD valve is closed.

The above test results further confirm that the FSD valve needs to move a certain distance before opening, indicating a delay in the opening process. Therefore, when the

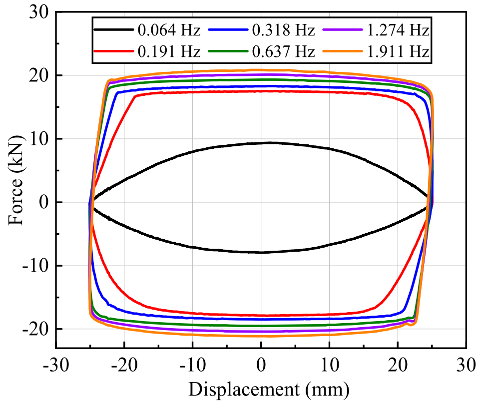

(a) Hysteresis curve of the conventional damper

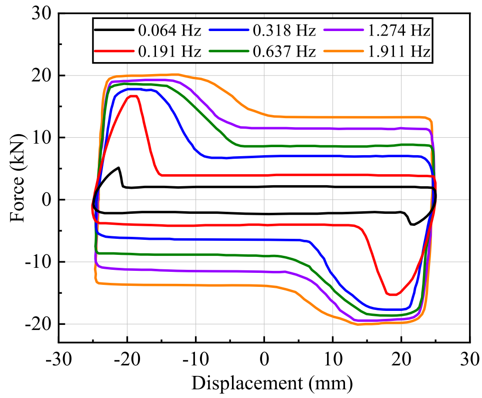

(b) Hysteresis curve of the FSD damper

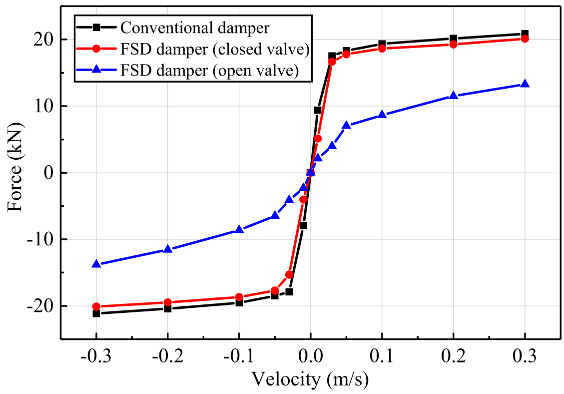

(c) Force-velocity characteristic curve

Figure 2. Comparison of the static characteristics of the conventional damper and FSD damper. (a) Hysteresis curve of the conventional damper; (b) Hysteresis curve of the FSD damper; (c) Force-velocity characteristic curve.

piston stroke of the damper is less than 1.0 mm, even at low frequencies, the FSD valve remains closed. This is because, on the one hand, the damping force is small in this condition, and on the other hand, the amplitude of the auxiliary piston is small, which is insufficient to open the FSD valve. When the excitation amplitude exceeds 1.0 mm, the frequency-dependent characteristics of the FSD damper become more significant. This also verifies that the switching frequency of the tested FSD damper is about 2–3 Hz. When the action frequency is less than 2 Hz, the FSD valve opens, resulting in a small damping force. Accordingly, if the action frequency is higher than 3 Hz, the FSD valve remains closed, resulting in a large damping force. That is consistent with the characteristics of conventional dampers.

3.3. Damping variation rate

The damping force variation of the FSD damper is mainly represented through hysteresis curves. To better evaluate the damping force reduction, in addition to comparing the

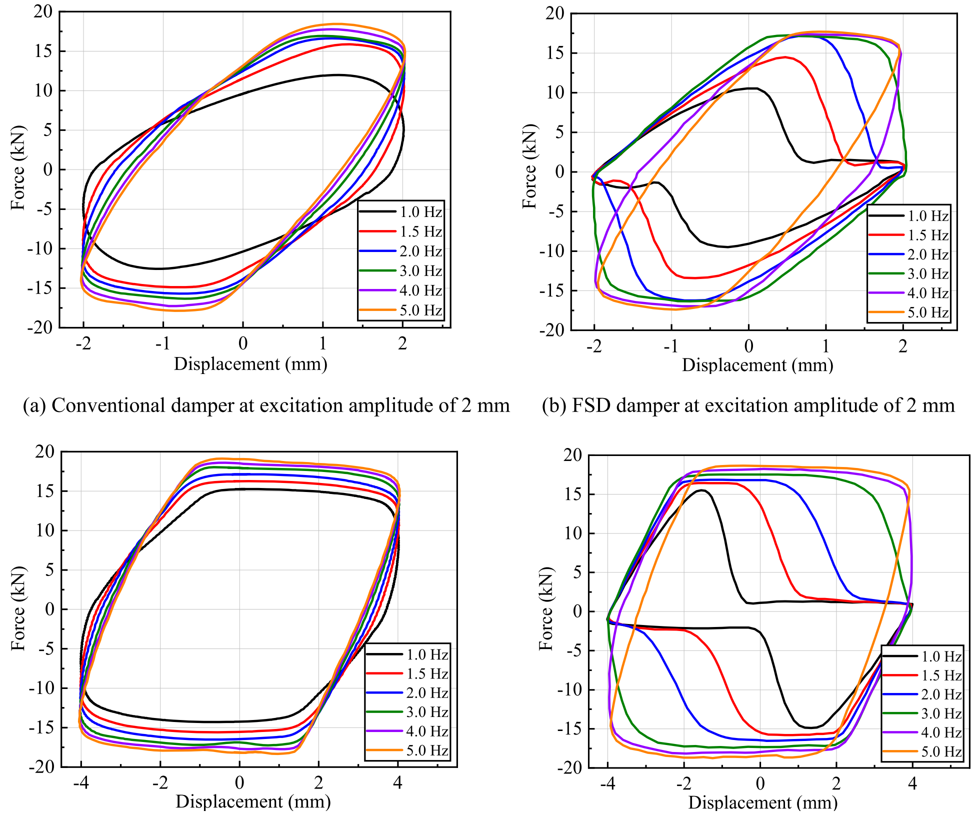

(a) Conventional damper at excitation amplitude of 2 mm (b) FSD damper at excitation amplitude of 2 mm

(c) Conventional damper at excitation amplitude of 4 mm (d) FSD damper at excitation amplitude of 4 mm

Figure 3. Force-displacement hysteresis curve of the yaw damper dynamic testing. (a) Conventional damper at excitation amplitude of 2 mm; (b) FSD damper at excitation amplitude of 2 mm; (c) Conventional damper at excitation amplitude of 4 mm; (d) FSD damper at excitation amplitude of 4 mm.

hysteresis curve, the concept of Damping Variation Rate (DVR) η is proposed. As shown in Figure 4(a), x_a is twice the amplitude of the static sinusoidal excitation. x_{fr} is the distance in the rebound stroke with low damping force due to the FSD valve opening, and x_{fc} is the corresponding distance in the compression stroke. The DVR is defined as

$$\begin{cases} \eta_r = \dfrac{x_{fr}}{x_a} \\ \eta_c = \dfrac{x_{fc}}{x_a} \\ \eta = \dfrac{\eta_r + \eta_c}{2} \end{cases} \tag{1}$$

where η_r and η_c represent the DVR during the rebound stroke and compression stroke, respectively, and η represents the average DVR. The η is a dimensionless quantity, theoretically ranging from 0 to 100%. A higher η indicates more significant frequency sensitivity.

The DVR in the static test versus frequency is shown in Figure 4(b), in which the DVR gradually decreases from 90% at 0.064 Hz to 50% at 1.911 Hz as the action frequency

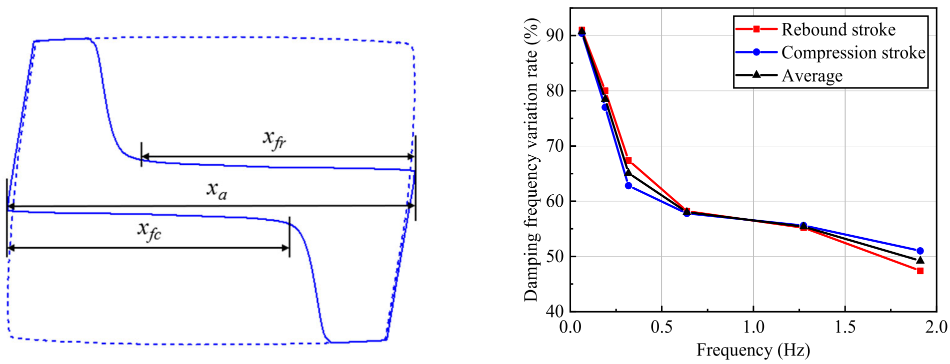

(a) Schematic diagram of calculation method (b) Static tested DVR of the FSD damper

Figure 4. Damping variation rate. (a) Schematic diagram of calculation method; (b) Static tested DVR of the FSD damper.

increases. This indicates that the response of the FSD valve opening slows down, and the characteristics of the damper tend towards those of a conventional type.

4. Modelling and simulation of FSD yaw damper

A simulation model for the yaw damper was established in the software of AMESim and the results were compared with the bench test results from Section 3 to verify the simulation accuracy. Then, the influences of key parameters of the FSD valve on mechanical characteristics of the FSD yaw damper were investigated.

4.1. AMESim simulation model

AMESim is an integrated multidisciplinary system modelling and simulation software primarily used for modelling and simulating mechanical, hydraulic, control systems and more. For the structure and operational principle of the double-cycle yaw damper introduced in Section 2, a physical parameter model is established in AMESim [20]. First, the model of the FSD valve is created as shown in Figure 5. It includes several components such as an auxiliary piston mass, a first and a second auxiliary chamber, a spring, a constant orifice and two check valves. The model can simulate the motion of the auxiliary piston under the action of the oil pressure from the damper's rebound or compression chamber.

The key parameters of the FSD valve are set as shown in Table 1. The lower diameter d_{c2} and mass m_c of the auxiliary piston are limited by structure space, which can be considered unchangeable. The auxiliary piston upper diameter d_{c1}, the boss height h_c, the constant orifice diameter d_{c3}, the spring stiffness K_d and the spring preload force F_{pre} shown in Figure 1(c) can be analysed to illustrate their influence laws on the mechanical characteristics of the damper.

Integrating the FSD valve into the conventional double-cycle damper model, the FSD damper was established as shown in Figure 6. Without altering the original structure of

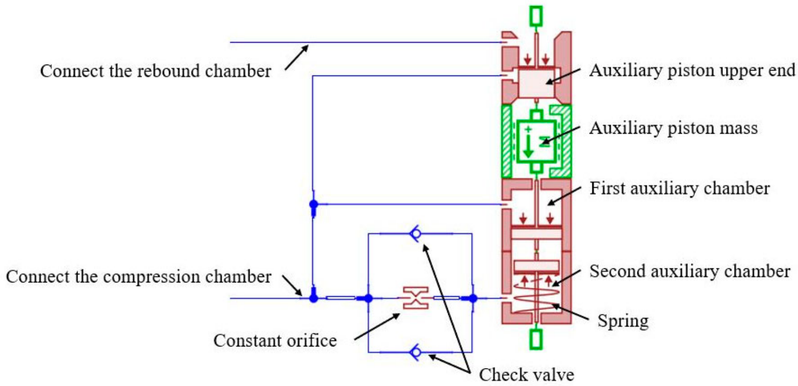

Figure 5. AMESim simulation model of FSD valve.

Table 1. Initial parameter settings for the AMESim model of FSD valve.

Component parameters	Value	Unit
Auxiliary piston upper diameter d_{c1}	12	mm
Auxiliary piston lower diameter d_{c2}	20	mm
Boss height h_c	1.4	mm
Constant orifice diameter d_{c3}	0.2	mm
Spring stiffness K_d	60	N/mm
Spring preload force F_{pre}	60	N
Auxiliary piston mass m_c	30	g

the conventional damper, two FSD valves are arranged in rebound and compression directions, respectively. Generally, there are three conventional rebound damping valves, one rebound FSD valve, three conventional compression damping valves and one compression FSD valve, constituting a total of eight damping valves on the piston. The main parameters of the conventional double-cycle damper are presented in Appendix.

4.2. Verification of static characteristics

According to the damper static test conditions, the simulated and measured hysteresis curves of the static characteristic are shown in Figure 7(a). It can be observed that the hysteresis curves are symmetrical during rebound and compression strokes, and there is a noticeable reduction in the damping force, indicating that the FSD valve is open. Additionally, as the excitation frequency increases, the delay during the opening process of the FSD valve increases. At 1.237 Hz, the faster opening of the FSD valve in the simulation model leads to a more rapid transition from the high damping force to the low force due to the modelling simplification of conventional damping valves and the neglect of factors such as friction, oil leakage and so on. In addition, the simulated hysteresis curves are less smooth in the transition area and exhibit some peaks. Figure 7(b) shows the comparison of DVR between simulated and test results. Both of them display a similar trend of decreased DVR with increasing frequency, from 90% at 0.064 Hz to 50% at 1.911 Hz. Due to the dispersion of experimental samples and the neglect of certain non-ideal factors in the simulation

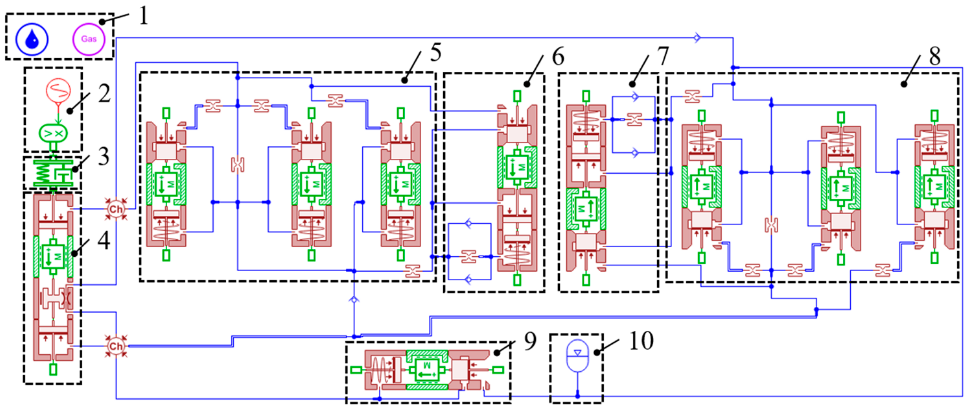

Figure 6. AMESim simulation model of the FSD damper. 1-Oil and gas properties; 2-External excitation; 3-Rubber joint; 4-Oil cylinder and piston; 5-Conventional rebound damping valves; 6-Rebound FSD valve; 7-Compression FSD valve; 8-Conventional compression damping valves; 9-Bottom check valve; 10-Reservoir chamber.

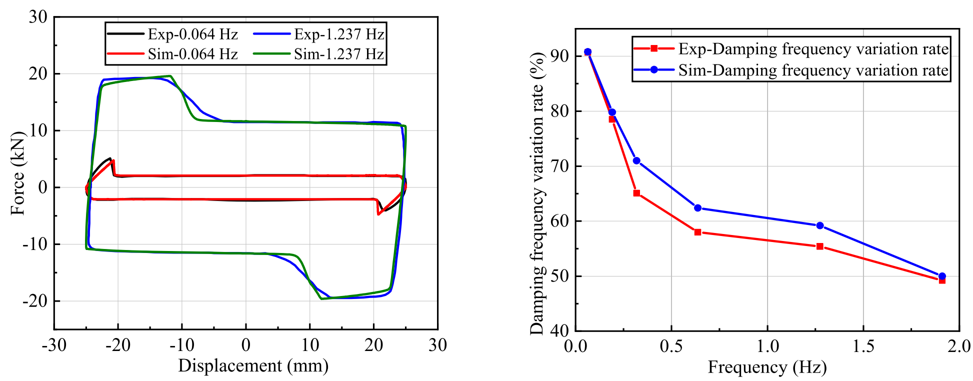

(a) Comparison of hysteresis curves

(b) Comparison of DVR

Figure 7. Verification of static characteristics of simulation model. (a) Comparison of hysteresis curves; (b) Comparison of DVR.

model, the simulated DVR is slightly higher than the experimental value at 0.318, 0.637 and 1.274 Hz, but the error is within 5%.

4.3. Verification of dynamic characteristics

Dynamic characteristic simulations refer to the damper dynamic test conditions. The hysteresis curves at four excitation amplitudes and two frequencies are shown in Figure 8. It can be observed that the simulated results align well with the measured data. At the excitation amplitude of 0.5 mm, the damper hysteresis curves take an elliptical shape without reaching the unloading force, and there are no noticeable reductions in the damping force, indicating that the FSD valves are closed. At the excitation amplitude of 1.0 mm, there is a

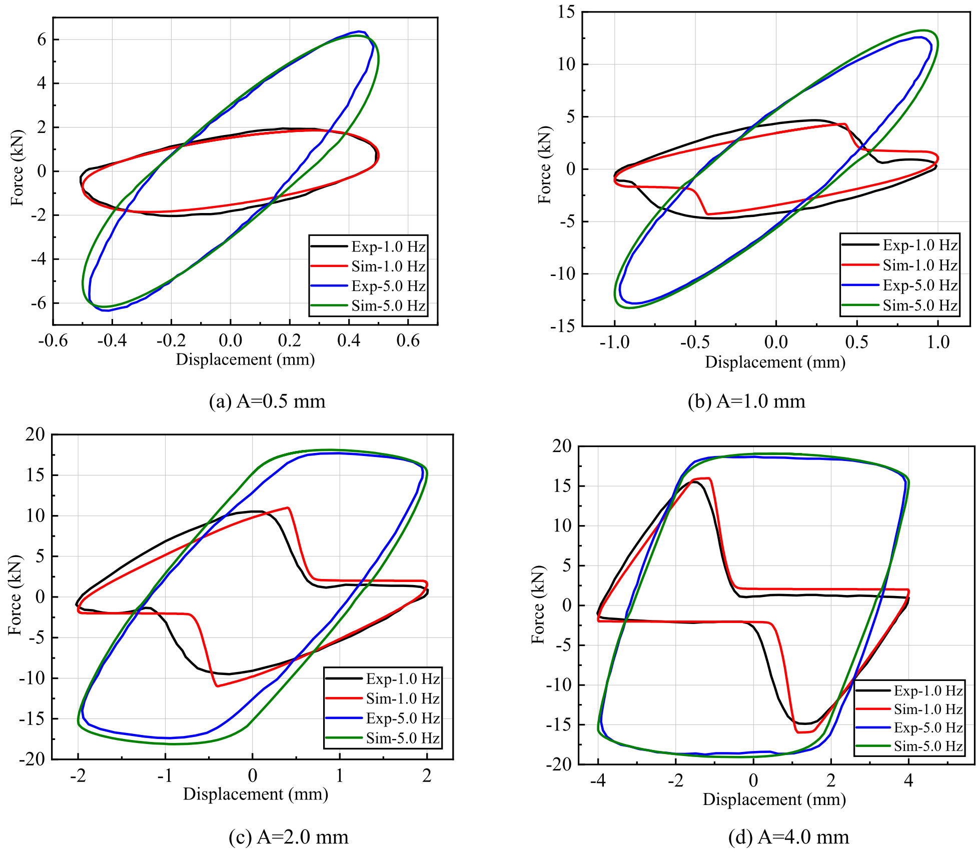

Figure 8. Verification of dynamic characteristics of simulation model. (a) A = 0.5 mm; (b) A = 1.0 mm; (c) A = 2.0 mm; (d) A = 4.0 mm.

noticeable reduction in the damping force at the frequency of 1 Hz. The hysteresis curves are completely elliptical at 5 Hz due to the closed FSD valve. The measured hysteresis curve at 1 Hz shows no decrease in the damping force during the compression stroke because the settings of the compression FSD valve differ from those of the rebound FSD valve, leading to asymmetry between the rebound and compression phases. However, the simulated one shows good symmetry in both rebound and compression directions along with an evident decrease in the damping force.

Figure 8(c) and (d) show that the damping forces reach the unloading force at excitation amplitudes of 2.0 and 4.0 mm, displaying a significant unloading phenomenon. Meanwhile, there is a noticeable reduction in the damping force at 1 Hz, indicating that the FSD valves are open. At 5 Hz, there are high damping forces in both rebound and compression strokes without force reduction. The simulation results align well with the measurement regarding the hysteresis curves.

In summary, the established AMESim model of the FSD damper accurately simulates both the static and dynamic characteristics, with which the impact of key parameters of the FSD valve on the damper mechanical characteristics can be researched more intensively.

5. The key parameters analysis of FSD valve

The key parameters of the FSD valve shown in Figure 1(c) include the boss height h_c, the auxiliary piston upper diameter d_{c1}, the constant orifice diameter d_{c3}, the spring stiffness K_d and the Spring preload force F_{pre}. The influence of the parameter variation on the mechanical characteristics of the FSD damper was investigated. The simulations are conducted under the sinusoidal excitation condition at an amplitude of 25 mm and a frequency of 0.637 Hz.

Keeping the value of d_{c1}, d_{c3}, K_d and F_{pre} as a constant, the boss height h_c is varied from 0.6 to 2.6 mm. Taking the rebound FSD valve in one cycle as an example, the displacement of the auxiliary piston and the flow volume of the FSD valve in time domain with different h_c are shown in Figure 9(a) and (b). The static hysteresis curves of the FSD damper with different h_c are shown in Figure 9(c). When the displacement of the auxiliary piston exceeds h_c, the flow volume of the FSD valve occurs, and there is a flow shock at the beginning. The time of the FSD valve opening increases with h_c. However, the time of the FSD valve closing is not significantly affected by h_c. This is because during the closing process, the check valve opens to ensure that the auxiliary piston moves quickly. With the increase of h_c, the delay of the FSD valve opening increases, and the damping force increases after the valve opens, indicating that the boss height affects the response of the FSD valve opening.

Similarly, the influence of the auxiliary piston upper diameter d_{c1}, the constant orifice diameter d_{c3}, the spring stiffness K_d and the spring preload force F_{pre} on the mechanical characteristics of the FSD damper have been analysed. Their corresponding hysteresis curves are shown in Figure 10. The larger d_{c1}, the faster the FSD valve opens and the smaller the damping force after the valve opens. The delay of the FSD valve opening decreases with increasing constant orifice diameter d_{c3}, while the damping force remains unaffected after the valve opens. The constant orifice provides motion damping for the auxiliary piston and affects its response time instead of the maximum displacement. The hysteresis curves corresponding to different spring stiffness K_d and spring preload force F_{pre} are shown in Figure 10(c) and (d). The larger the K_d and F_{pre}, the greater the delay and the damping force after the FSD valve opens. Taking the structural implementation and performance requirements into account, the key parameters of the FSD valve can be adjusted through simulation and physical tuning.

6. The simulation of vehicles dynamic performances

This Section mainly analyses the impact of the FSD yaw damper on the dynamics performance of railway vehicles. Compared to the conventional yaw damper, the dynamics performance of a high-speed locomotive employing the FSD yaw damper in different line conditions and wheel–rail matching states were simulated. Moreover, the optimisation analysis of the key parameters of the FSD valve was conducted.

6.1. Vehicle-damper co-simulation dynamics model

Taking a type of high-speed locomotive with Bo'-Bo' axle arrangement as the simulation object [21], the dynamics model was established using the multibody system dynamics software Simpack, as shown in Figure 11. The rigid bodies consist of 1 carbody, 2 frames,

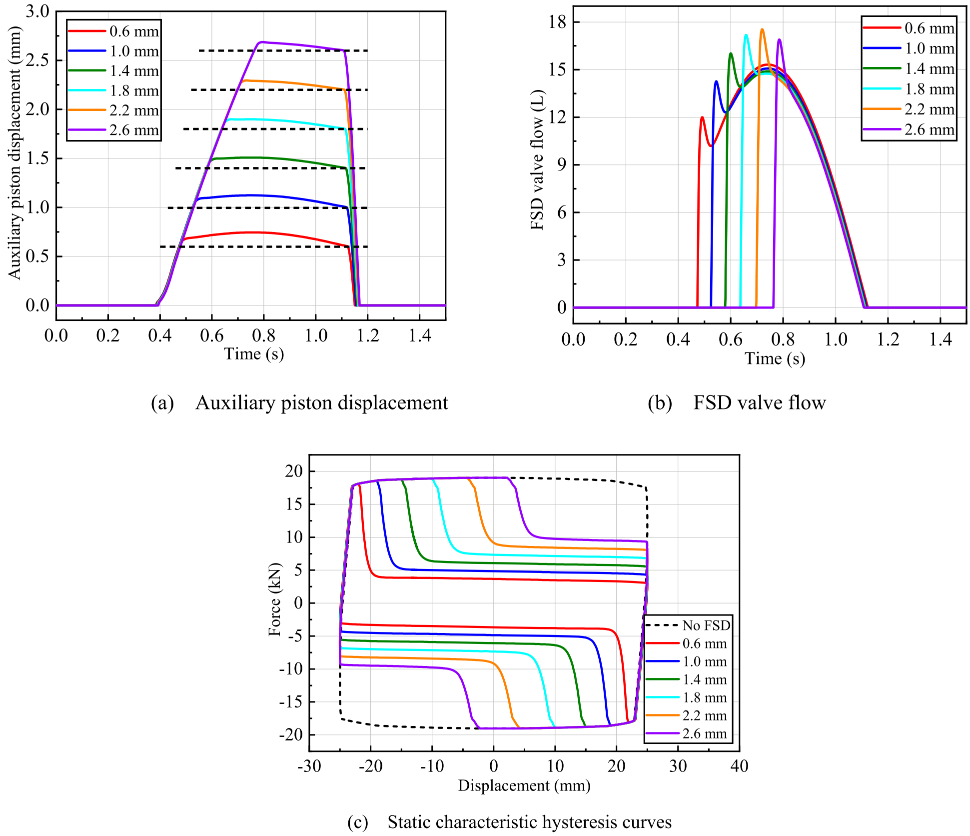

Figure 9. Calculation results of different boss heights. (a) Auxiliary piston displacement; (b) FSD valve flow; (c) Static characteristic hysteresis curves.

2 traction rods, 4 wheelsets, 4 motors, 4 hollow shafts and 8 rotary arm axle-boxes. The model has a total of 90 degrees of freedom (DOFs). The wheelset, motor, bogie and carbody all have 6 DOFs. The hollow shaft has 3 DOFs, including lateral, roll and yaw motions relative to the wheelset. The traction rod has 2 DOFs, namely yaw and pitch relative to the carbody. The axle-box has 1 DOF and rotates around the wheelset. The main dynamic parameters of the locomotive are presented in Appendix.

A total of four FSD yaw dampers were modelled in the AMESim software. Co-simulation of the two different models was communicated with MATLAB/Simulink. In every integration step, the relative displacement of the yaw damper in Simpack is transmitted to AMESim, in which the output force of the damper is calculated timely and then transmitted back to Simpack, thereby realising the close loop of data interaction for the co-simulation.

The centralised power EMUs can operate across the high-standard and existing low-speed railways, so their operating line conditions are more severe, and the wheel–rail relationship is more complex, resulting in more severe dynamic problems. The range of the nominal equivalent conicity λ_e at 3 mm wheelset lateral displacement is relatively large, even up to 0.9. Previous studies have shown that the high-speed locomotive is prone to

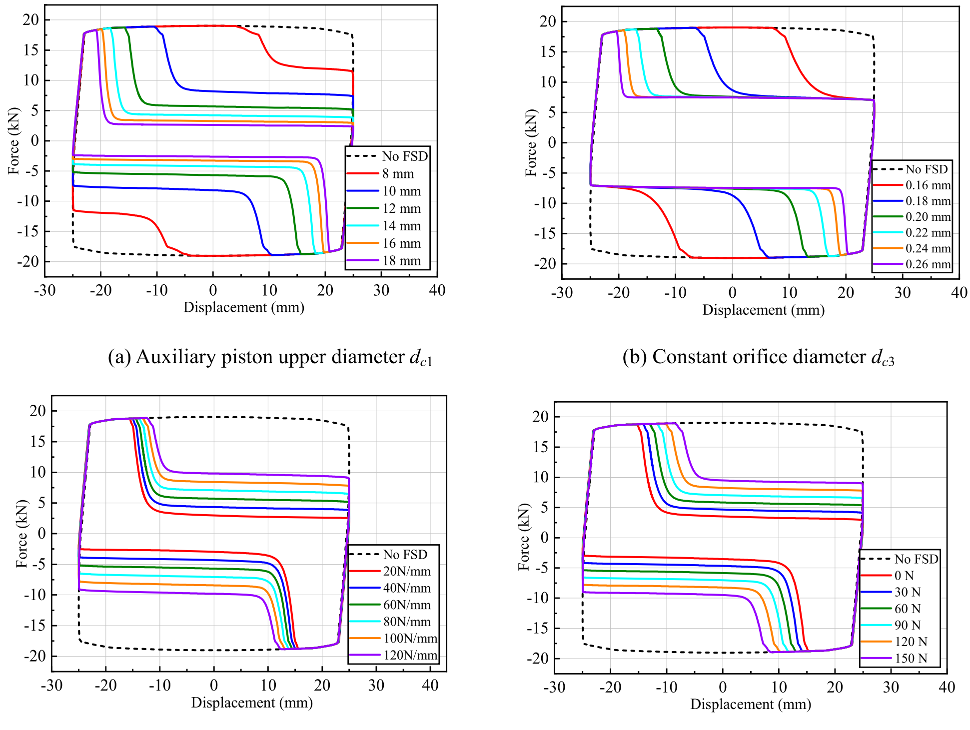

(a) Auxiliary piston upper diameter d_{c1}

(b) Constant orifice diameter d_{c3}

(c) Spring stiffness K_d

(d) Spring preload force F_{pre}

Figure 10. Hysteresis curve of FSD damper with different parameters. (a) Auxiliary piston upper diameter d_{c1}; (b) Constant orifice diameter d_{c3}; (c) Spring stiffness K_d; (d) Spring preload force F_{pre}.

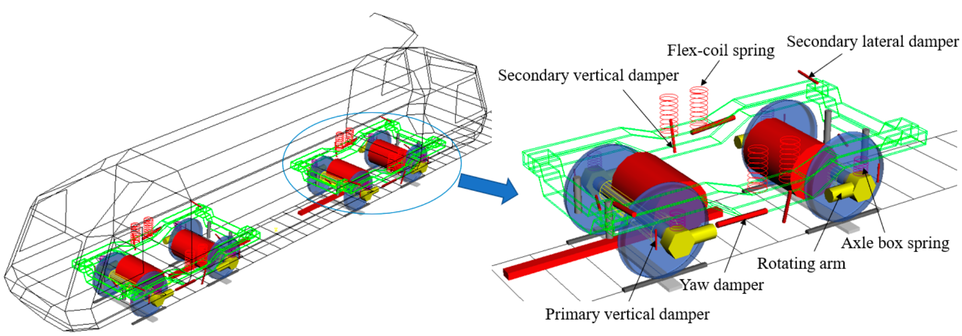

Figure 11. The dynamics model of high-speed locomotive.

low-frequency swaying in low-conicity conditions, and as the wheel tread wears, intense bogie hunting occurs in high-conicity conditions [22–25]. In order to comprehensively simulate the actual operating conditions of the high-speed locomotive, three types of wheel profiles are adopted to cover the range of equivalent conicity variation on actual operating. The rail adopts the standard CHN60 profile, and the rail cant is set to 1:40. The equivalent conicity values at the 3 mm lateral displacement corresponding to the wheel–rail contact states of low-conicity, normal-conicity and high-conicity are 0.04, 0.10 and 0.70,

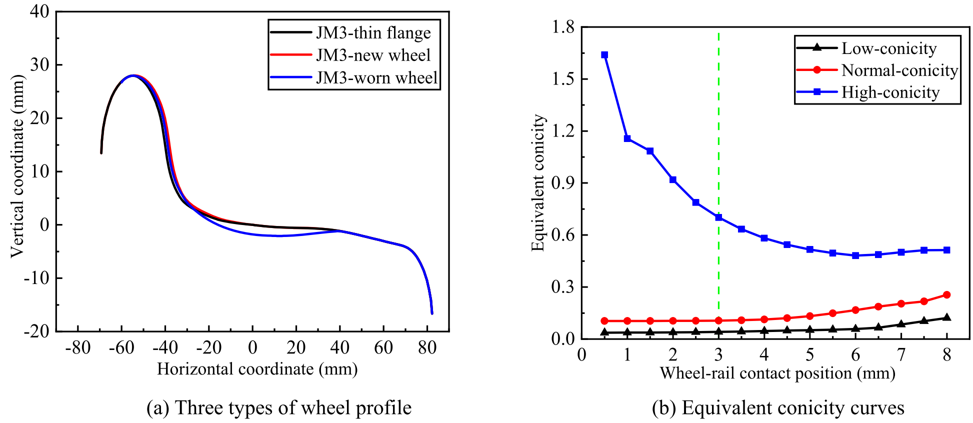

Figure 12. Three types of wheel-rail geometric matching. (a) Three types of wheel profile; (b) Equivalent conicity curves.

respectively. The equivalent conicity curves of the three types of wheel profiles are shown in Figure 12 [11].

6.2. The adaptability to wheel–rail relationship

When the equivalent conicity of wheel–rail matching is too low or too high, the dynamic performance of the high-speed locomotive deteriorates severely. Therefore, a low-conicity condition and a high-conicity condition are mainly considered in the simulation. The length of the straight track is set to 800 m, and the track excitation adopts the measured irregularity of the Wuhan–Guangzhou high-speed railway [26]. The locomotive running speed is 200 km/h. In order to highlight the advantages of the FSD yaw damper, it is compared with a conventional damper with a small damping of 200 kN·s/m (referred to as C200) and a damper with a large damping of 800 kN·s/m (referred to as C800). The parameters of the FSD valve are set according to Table 1. In the low-conicity condition, prominent carbody swaying is prone to occur. On the contrary, the bogie hunting motion is prone to occur in the high-conicity condition. Therefore, the lateral acceleration of the carbody is mainly analysed in the low-conicity condition, and the lateral acceleration of the bogie frame is mainly emphasised in the high-conicity condition.

6.2.1. Low-conicity condition

The simulation results of the carbody lateral acceleration with the three dampers in the low-conicity condition are shown in Figure 13. It can be known that the lateral acceleration of the carbody employing the C200 damper is the smallest, and the lateral acceleration of the carbody employing the C800 damper is the largest, while the lateral acceleration of the carbody employing the FSD damper is between the results of C200 and C800 dampers. The lateral ride indexes of the carbody with the three dampers are 2.322, 2.718 and 2.524, respectively. It can also be seen from the spectrum diagram in Figure 13(b) that the peak of the lateral acceleration of the carbody employing the FSD damper is 0.113 $(m/s^2)^2/Hz$, which is 56.9% lower than the peak of the carbody with the C800 damper. Therefore, the effect of the FSD yaw damper is similar to that of the small damping yaw damper in the

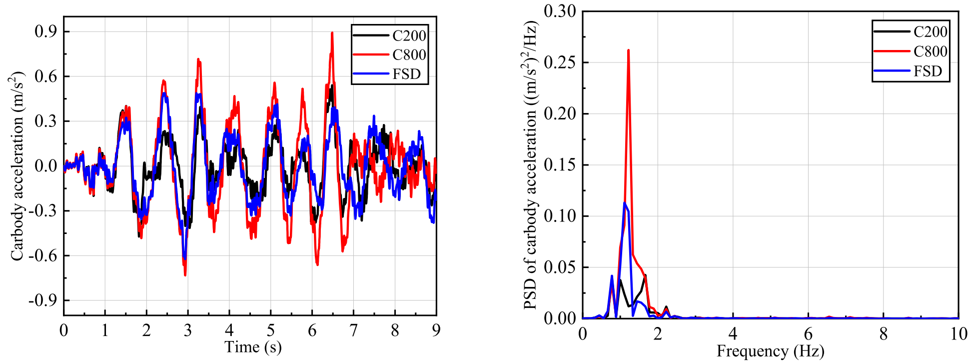

(a) Carbody acceleration in time domain (b) Carbody acceleration in frequency domain

Figure 13. Comparison of the carbody lateral acceleration in low-conicity condition. (a) Carbody acceleration in time domain; (b) Carbody acceleration in frequency domain.

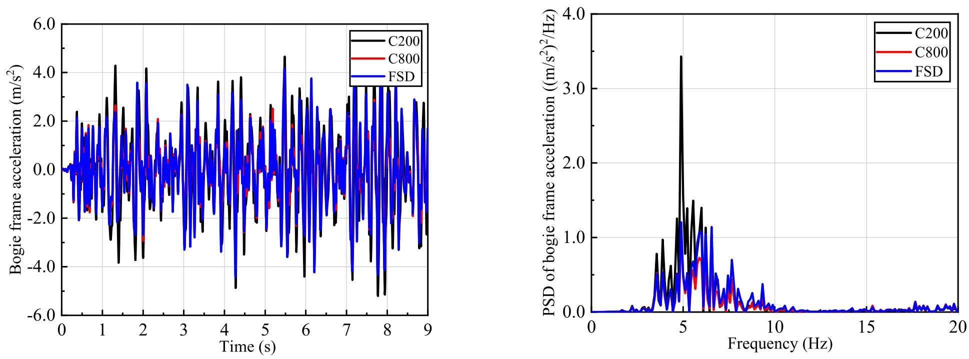

(a) Frame acceleration in time domain (b) Frame acceleration in frequency domain

Figure 14. Comparison of the bogie frame lateral acceleration in high-conicity condition. (a) Frame acceleration in time domain; (b) Frame acceleration in frequency domain.

low-conicity condition, significantly reducing carbody lateral swaying and improving the ride comfort.

6.2.2. High-conicity condition

The simulation results of the frame lateral acceleration with the three dampers in the high-conicity condition are shown in Figure 14. It can be known that the lateral acceleration of the bogie frame employing the C200 damper is the largest, and the lateral acceleration of the bogie frame employing the FSD damper is basically the same as the locomotive with the C800 damper. The frame acceleration with the three dampers is 5.375, 4.123 and 4.394, respectively. It can also be seen from Figure 14(b) that the peak of the frame lateral acceleration with the FSD damper is 1.206 $(m/s^2)^2/Hz$, which is 64.8% lower than that of the locomotive with the C200 damper. Therefore, the effect of the FSD yaw damper is similar to that of the large damping yaw damper in the high-conicity condition, which can significantly reduce the frame lateral vibration acceleration and improve bogie hunting stability.

Table 2. Lateral dynamic performance of locomotive with different boss height h_c.

	Lateral ride index of carbody		Bogie frame lateral acceleration (m/s^2)	
Boss height (mm)	Low-conicity	High-conicity	Low-conicity	High-conicity
0.6	2.468	2.017	1.827	4.710
1.0	2.487	2.100	1.803	4.528
1.4	2.524	2.131	1.736	4.394
1.8	2.653	2.132	1.753	4.254
2.2	2.687	2.132	1.793	4.254
2.6	2.715	2.132	1.747	4.254

To sum up, the FSD yaw damper can balance the lateral stability of the locomotive in a wide range of wheel–rail matching states, to enhance the vehicle adaptive stability, improving the robustness to wheel–rail relationships and extending the repairing cycle of tread profiles.

6.3. Key parameters of FSD valve

It can be known from Section 5 that changing the structural parameters of the FSD valve has a significant impact on the damping force of the damper. For instance, increasing the boss height h_c prolongs the opening time of the auxiliary piston and thus increases the damping force of the yaw damper, which is unfavourable for the carbody stability in the low-conicity condition while favourable for reducing the lateral vibration acceleration of the bogie frame in the high-conicity condition. Table 2 shows the calculation results of the lateral dynamic performance of the locomotive with h_c varying from 0.6 to 2.6 mm. With the increase of h_c, the lateral ride index of the locomotive gradually increases in the low-conicity condition, while the lateral acceleration of the bogie frame significantly decreases in the high-conicity condition, changing from 4.710 to 4.254 m/s^2. The above simulation results suggest that the requirements for the h_c are contradictory in the high-/low-conicity conditions. Similarly, the influence of other parameters of the FSD valve on the vehicle dynamic performance can be obtained through simulations, so as to reasonably select the appropriate value according to the specific requirements. The influences of d_{c1}, d_{c3}, K_d and F_{pre} on the vehicle dynamic performance in different wheel–rail contact states will not be elaborated.

6.4. Narrow curve passing

In addition to improving the adaptive lateral stability of railway vehicles to the various wheel–rail geometric matching, the FSD yaw damper can also reduce the wheel guiding force, derailment coefficient, and other indicators when the vehicle passes through a lateral turnout and a narrow curve. In this Section, an S-shaped curve of lateral turnout is set to compare the difference of the narrow curve passing performance of the locomotive between employing the conventional and the FSD yaw damper. The S-shaped curve consists of two reverse curves without transition. The radius of the reverse curves is 190 m and the length of the embedded line is 6 m [27,28]. The standard wheel profile with the nominal equivalent conicity of 0.10 is adopted. The total length of the track is set to 120 m without track irregularities, and the passing speed is 43 km/h.

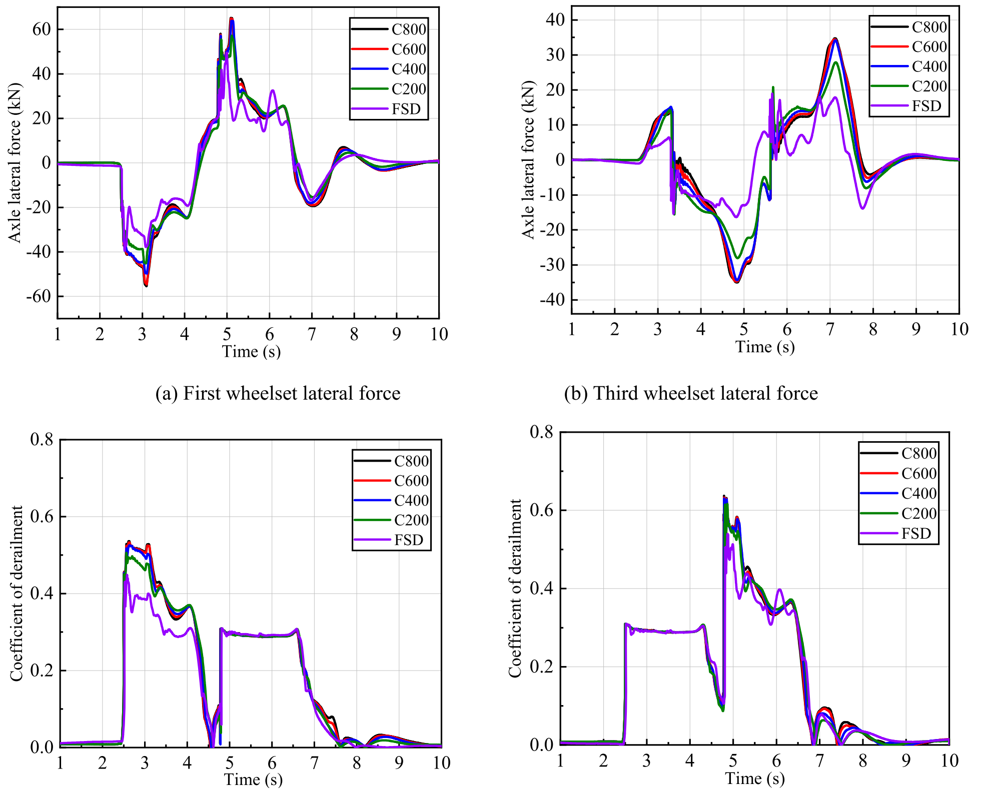

(a) First wheelset lateral force
(b) Third wheelset lateral force
(c) Left wheel Y/Q of first wheelset
(d) Right wheel Y/Q of first wheelset

Figure 15. Simulation results of the locomotive S-curve passing. (a) First wheelset lateral force; (b) Third wheelset lateral force; (c) Left wheel Y/Q of first wheelset; (d) Right wheel Y/Q of first wheelset.

The time-domain curves of the lateral force of the first and the third wheelsets are extracted as shown in Figure 15(a) and (b). The wheelset lateral force of the locomotive employing the original C800 yaw damper is the largest, and the lateral force of the first wheelset is greater than that of the third wheelset. When the damping coefficient of the conventional damper changes from 800 kN·s/m to 200 kN·s/m, the reduction of the wheelset lateral force is obvious. However, this still cannot achieve the significant effects of the FSD yaw damper. After adopting the FSD damper, the lateral force of the first wheelset is reduced from 65.20 to 49.60 kN, decreasing by 23.93%. The wheelset lateral force of the third wheelset is reduced from 35.04 to 18.95 kN, with a decrease of 45.92%.

The time-domain curves of the derailment coefficient Y/Q of the first wheelset are extracted as shown in Figure 15(c) and (d). After adopting the FSD damper, the Y/Q of the first wheelset is reduced from 0.637 to 0.539, with a decrease of 15.38%, and the Y/Q of the third wheelset is reduced from 0.486 to 0.405, with a decrease of 16.67%. The indicators in the S-curve passing condition with five different types of yaw dampers are shown in Table 3. To sum up, the FSD yaw damper can effectively improve the locomotive dynamic performance of narrow curves passing.

Table 3. Simulation results of S-curve passing of locomotive with different dampers.

Damper model	FR-Damper force (kN)	BR-Damper force (kN)	First wheelset force (kN)	Third wheelset force (kN)	First wheelset Y/Q	Third wheelset Y/Q
C800	20.58	19.30	65.20	35.04	0.637	0.486
C600	20.53	19.21	64.96	34.74	0.633	0.484
C400	20.53	18.98	63.89	34.35	0.630	0.477
C200	20.03	16.46	57.21	28.04	0.617	0.438
FSD	15.28	8.12	49.60	18.95	0.539	0.405

7. Conclusions

(1) The frequency-selective damping (FSD) valve is a key component in the damper to achieve the damping force variation according to the action frequency. The valve closes in high-frequency operating conditions, which makes the mechanical characteristics of the damper consistent with those of conventional dampers, maintaining a large damping force. On the contrary, the valve opens to decrease the damper output force at a frequency below 2–3 Hz. The opening or closing of the FSD valve is automatically switched by its internal mechanical structure. The damper is suitable for railway vehicles requiring different damping forces in different frequency ranges.

(2) The static and dynamic characteristic tests were conducted to compare the differences between the conventional and the FSD dampers. The FSD damper shows a significant reduction in the damping force at low frequencies compared to the conventional damper, indicating a noticeable opening of the FSD valve. However, because the opening of the FSD valve needs to meet certain requirements, the delay of valve opening causes the force-displacement hysteresis curve to be no longer a standard ellipse or an approximate parallelogram caused by unloading. The concept of damping variation rate (DVR) is proposed to evaluate the degree of damping force reduction for the FSD damper. With increasing action frequency, the DVR gradually decreases to 0 and the characteristics of the FSD damper approximate those of the conventional one.

(3) A physical parameter model of the hydraulic damper is established in the AMESim software, and the simulation accuracy has been verified by comparing the simulated results to the measurements. The influences of key parameters of the FSD valve are studied in the condition of low-frequency and large-amplitude sinusoidal excitations. The results show that increasing the upper diameter of the auxiliary piston d_{c1} and constant orifice diameter d_{c3}, decreasing the spring stiffness K_d and preload force F_{pre}, as well as the boss height h_c, are beneficial for improving the response speed of the FSD valve, thereby enhancing the sensitivity of frequency-dependent damping.

(4) The dynamics co-simulation of a locomotive and four FSD yaw dampers in different wheel–rail contact conditions have been implemented with the AMESim and the Simpack software. The results verify that the FSD damper improves the adaptive hunting stability of the locomotive in a wider range of wheel–rail matching conicity. In addition, in the simulation of a S-curve passing, the wheelset lateral force and derailment coefficient of the locomotive employing the FSD yaw damper are

significantly reduced, indicating that the FSD damper can also improve the vehicle dynamic performance of narrow curves passing.

(5) Temperature has a significant effect on the behaviour of hydraulic dampers. In future research, it's essential to investigate the characteristic variation of the FSD damper with temperature and establish a damper model capable of considering its effect. Moreover, the FSD damper may can also replace other conventional hydraulic dampers in suspension systems, such as the secondary lateral damper, to improve the vehicle performance, depending on the influence law of considered suspension damping.

Disclosure statement

No potential conflict of interest was reported by the author(s).

Funding

The material in this paper is based on work supported by the National Natural Science Foundation of China [grant numbers 52372403; U2268211], the Natural Science Foundation of Sichuan Province [grant numbers 2022NSFSC0034] and the National Railway Group Science and Technology Program [grant number N2023J071].

ORCID

Yuan Yao http://orcid.org/0000-0003-2279-7463

References

[1] Gao HX, Chi MR, Dai LC, et al. Mathematical modelling and computational simulation of the hydraulic damper during the orifice-working stage for railway vehicles. Math Probl Eng. 2020;2020:1–23.

[2] Shen LJ, Wang S, Chen ZQ, et al. Numerical simulation and experimental study of electromagnetic eddy current damper for railway vehicles. J Railw Sci Eng. 2022;19(5):1433–1441.

[3] Zong LH, Gong XL, Xuan SH, et al. Semi-active H^{∞} control of high-speed railway vehicle suspension with magnetorheological dampers. Veh Syst Dyn. 2013;51(5):600–626. doi:10.1080/00423114.2012.758858

[4] Wang DH, Liao WH. Semi-active suspension systems for railway vehicles using magnetorheological dampers. Part II: simulation and analysis. Veh Syst Dyn. 2009;47(12):1439–1471. doi:10.1080/00423110802538336

[5] Zhang XG, Zhou Y, Jiang C, et al. Modeling and simulation of lateral fuzzy control semi-active suspension system for high-speed trains considering time delay compensation. J Railw Sci Eng. 2023;20(4):1189–1199.

[6] Lee CT, Moon BY. Simulation and experimental validation of vehicle dynamic characteristics for displacement-sensitive shock absorber using fluid-flow modelling. Mech Syst Signal Pr. 2006;20(2):373–388. doi:10.1016/j.ymssp.2004.09.006

[7] Nie SD, Zhuang Y, Wang Y, et al. Velocity & displacement-dependent damper: a novel passive shock absorber inspired by the semi-active control. Mech Syst Signal Pr. 2018;99:730–746. doi:10.1016/j.ymssp.2017.07.008

[8] Paul DK. Frequency-selective damper valve, and shock absorber and piston having such valve. US10830304. 2020-11-10.

[9] Marcin K, Karol P. Hydraulic damper having a high frequency valve assembly. EP3396198. 2021-04-21.

[10] Łuczko J, Ferdek U. Nonlinear dynamics of a vehicle with a displacement-sensitive mono-tube shock absorber. Nonlinear Dyn. 2020;100(1):185–202. doi:10.1007/s11071-020-05532-7

[11] Li G, Zhou Y, Yao Y, et al. Application of yaw dampers with frequency-selective damping to improve the locomotive adaptability to low/high conicity stability. Proc Inst Mech Eng Part F-J Rail Rapid Transit. 2023;237(6):784–795. doi:10.1177/09544097221141517
[12] Decock P. Fluid-filled frequency dependent damper. CN201280054137.4. 2016-05-04.
[13] Cheng J, Li G, Yan HW, et al. Simulation research on the application of frequency-selective-damper for low frequency swaying of locomotive. J Dyn Control. 2022;20(02):71–77.
[14] Huo WB, Yue BS, Liu XG, et al. The development of stiffness-adjustable anti-yaw damper. 26th Symposium of the International Association of Vehicle System Dynamics (IAVSD), Gothenburg, Sweden, August 2019.
[15] Yao Y, Chen XW, Li H, et al. Suspension parameters design for robust and adaptive lateral stability of high-speed train. Veh Syst Dyn. 2023;61(4):943–967. doi:10.1080/00423114.2022.2062012
[16] Isacchi G, Ripamonti F, Corsi M. Innovative passive yaw damper to increase the stability and curve-taking performance of high-speed railway vehicles. Veh Syst Dyn. 2023;61(9):2273–2291. doi:10.1080/00423114.2022.2105242
[17] Huang CH, Zeng J. Dynamic behaviour of a high-speed train hydraulic yaw damper. Veh Syst Dyn. 2018;56(12):1922–1944. doi:10.1080/00423114.2018.1439588
[18] Richard VK. A new shock absorber model for use in vehicle dynamics context. Veh Syst Dyn. 2005;43(9):613–631. doi:10.1080/0042311042000266720
[19] EN 13802:2013. Railway applications - suspension components - hydraulic dampers. Brussels: CEN; 2013.
[20] Ding WS, Ye YJ. Modeling and simulation of train hydraulic damper based on AMESim. Mach Tool Hydraul. 2009;37(9):213–215.
[21] Li G, Wu RD, Deng XX, et al. Suspension parameters matching of high-speed locomotive based on stability/comfort Pareto optimization. Veh Syst Dyn. 2022;60(11):3848–3867. doi:10.1080/00423114.2021.1979602
[22] Huang CH, Zeng J, Liang SL. Carbody hunting investigation of a high speed passenger car. J Mech Sci Technol. 2013;27:2283–2292. doi:10.1007/s12206-013-0611-z
[23] Bideleh S, Berbyuk V, Persson R. Wear/comfort Pareto optimisation of bogie suspension. Veh Syst Dyn. 2016;54(8):1053–1076. doi:10.1080/00423114.2016.1180405
[24] Sun JF, Chi MR, Jin XS, et al. Experimental and numerical study on carbody hunting of electric locomotive induced by low wheel-rail contact conicity. Veh Syst Dyn. 2021;59(2):203–223. doi:10.1080/00423114.2019.1674344
[25] Wei L, Zeng J, Chi MR, et al. Carbody elastic vibrations of high-speed vehicles caused by bogie hunting instability. Veh Syst Dyn. 2017;55:1321–1342. doi:10.1080/00423114.2017.1310386
[26] Li JY, Liu LY, Kou DH. Wu Guang high-speed rail track irregularity power spectrum analysis. Appl Mech Mater. 2014;638-640:1224–1228. doi:10.4028/www.scientific.net/AMM.638-640.1224
[27] En 14363:2016+A1 - railway applications - testing and simulation for the acceptance of running characteristics of railway vehicles - running behaviour and stationary tests. Brussels: CEN; 2016.
[28] Michalek T, Kohout M. On the problems of lateral force effects of railway vehicles in S-curves. Veh Syst Dyn. 2022;60(8):2739–2757. doi:10.1080/00423114.2021.1917631

Appendix

Table A1. Main parameters of the conventional yaw damper.

Parameter	Value	Unit
Oil density	830	Kg/m^3
Proportion of dissolved air in the oil	1	‰
Oil bulk modulus	17000	bar
Oil dynamic viscosity	0.0392	Pa·s
Diameter of piston	70	mm
Diameter of piston rod	30	mm
Length of the inner tube	340	mm
Diameter of constant orifice	0.45	mm
Spring stiffness of damping valve 1	90	N/mm
Preload of damping valve 1	60	N
Spring stiffness of damping valve 2	100	N/mm
Preload of damping valve 2	180	N
Spring stiffness of damping valve 3	280	N/mm
Preload of damping valve 3	300	N

Table A2. Main parameters of the high-speed locomotive.

Parameter	Value	Unit
Carbody mass	41900	kg
Bogie frame mass	3441	kg
Wheelset mass	2434	kg
Inertia moment of carbody about longitudinal/lateral/vertical axis	60/1322/1100	$t{\cdot}m^2$
Inertia moment of bogie frame about longitudinal/lateral/vertical axis	3739/8098/13488	$kg{\cdot}m^2$
Inertia moment of wheelset about longitudinal/lateral/vertical axis	1726/471/1726	$kg{\cdot}m^2$
Primary longitudinal stiffness	15	kN/mm
Primary lateral stiffness	3.5	kN/mm
Primary vertical stiffness	1.4	kN/mm
Primary vertical damping	60	kN·s/m
Secondary longitudinal stiffness	0.242	kN/mm
Secondary lateral stiffness	0.242	kN/mm
Secondary vertical stiffness	0.746	kN/mm
Secondary lateral damping	25	kN·s/m
Wheel base	2.9	m
Length between bogie centres	9	m
Wheel rolling radius	0.625	m